Pergamon

Int. J. Solids Structures Vol. 34, Nos 33-34, pp. 4357–4376, 1997

0020–7683/97 $17.00 + .00

PII: S0020–7683(97)00023–1

LONGITUDINAL AND FLEXURAL WAVE PROPAGATION IN REINFORCED CONCRETE COLUMNS

JUNYA YAMAKAWA and HIDENORI MURAKAMI†
Department of Applied Mechanics and Engineering Sciences, University of California at San Diego, La Jolla, California 92093-0411, U.S.A.

(*Received* 11 *September* 1996; *in revised form* 11 *December* 1996)

Abstract—In order to investigate elastic wave propagation in reinforced concrete (RC) columns with regular rebar arrangements, longitudinal and flexural phase velocity spectra of the Floquet-type harmonic waves were computed. Floquet's theorem was applied to the regularly reinforced RC columns to incorporate the heterogeneity induced by longitudinal steel bars, tie bars, and concrete. The numerical solution of phase velocity spectra was obtained by utilizing a semi-analytical finite element (FE) method. Phase velocity spectra exhibit strong dispersion similar to the Pochhammer and Chree problem of homogeneous circular cylinders. It was found that this dispersion in acoustic (lowest) modes was not accurately predicted by the elementary theories. However, it was found that the acoustic mode shapes of the Floquet waves can be closely approximated by plane sections, consistent with the assumptions of elementary rod and beam theories. The effect of transverse steel, in the form of tie bars, on phase velocity spectra of acoustic modes was found to be negligible due to the small volume fractions. In addition, by considering square and octagonal cross sections, the effects on dispersion of both cross sectional geometry and increasing volume fractions of longitudinal bars were investigated by neglecting tie bars. © 1997 Elsevier Science Ltd.

INTRODUCTION

In both the Northridge earthquake in 1994 and the Hyogoken Nanbu (Kobe) earthquake in 1995, fault rupture areas were located close to urban cities. As a result, a considerable number of reinforced concrete columns failed. In the Kobe earthquake, severe damage to reinforced concrete (RC) buildings was due to the failure of the columns: (i) in the first storey of the multistorey building with open retail space or parking and (ii) in a mid-level floor of mid-height storey buildings due to the abrupt stiffness changes (Architectural Institute of Japan, 1995; Shimizu Corporation, 1995). The ground motion close to the epicenter registered 818 gal (1 gal = 1 cm/s/s) in the north-south direction, 617 gal in the east-west direction, and 332 gal in the vertical direction (Architectural Institute of Japan, 1995). Extremely large vertical and horizontal accelerations create a high magnitude jolt which buildings experience in the same directions.

The objectives of the present paper are: (i) to obtain phase velocity spectra of harmonic waves in RC columns, (ii) to examine the accuracy of elementary rod and beam theories in simulating elastic wave propagation, and (iii) to investigate the effects of both cross sectional geometry and the volume fraction of longitudinal bars.

The wave propagation in an isotropic cylinder with a uniform circular cross section was analytically investigated by Pochhammer (1876) and Chree (1889). They predicted "wave dispersion" which means that harmonic wave velocity changes with wavelength or frequency. The dispersion spectra of the Pochhammer and Chree problems were numerically computed by Onoe, McNiven, and Mindlen (1962) for longitudinal waves and by Pao and Mindlin (1960) for flexural waves. The longitudinal wave propagation in composite circular cylinders having isotropic constituents was investigated by McNiven, Sackman, and Shah (1963) and Armenakas (1970). Semi-analytical finite element methods were employed for waveguide problems by Nelson *et al.* (1971), and Rattanawangcharoen *et al.* (1992) to investigate wave propagation in laminated-composite circular cylinders. In their analyses, the radial region was discretized into one-dimensional, two-node elements.

† Author to whom correspondence should be sent.

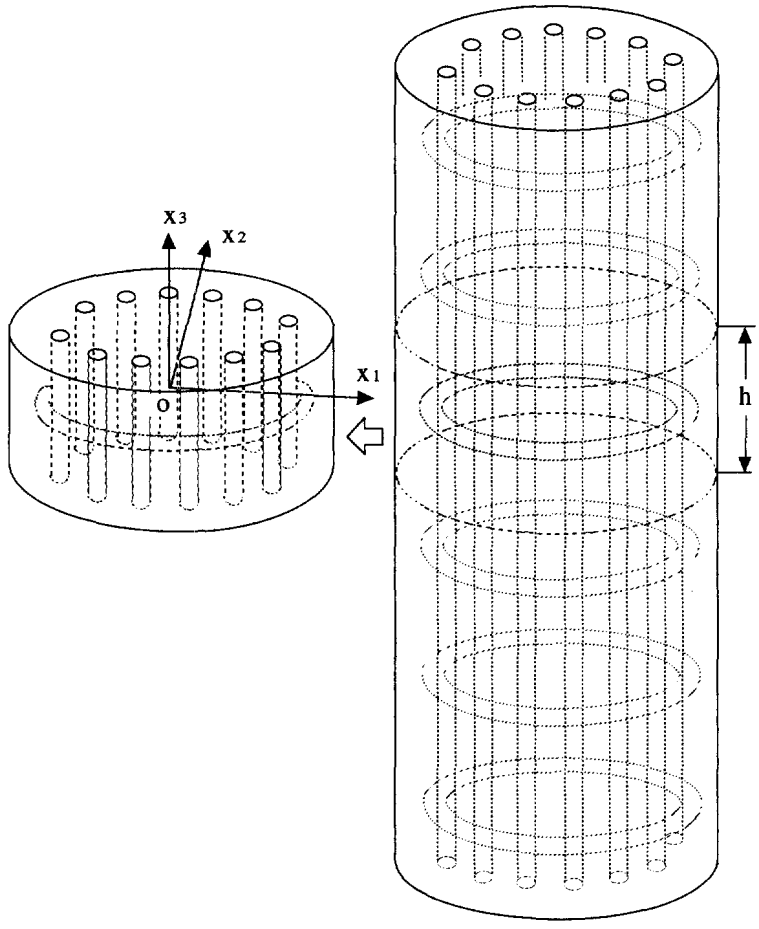

Fig. 1. An RC column with regular rebar arrangements and a unit cell.

The axial wave propagation in RC columns with regular rebar arrangements is a special case of elastic wave propagation in regularly heterogeneous materials. The regularly heterogeneous structure is described by a unit cell. In RC columns, the periodic cell-structure extends only in the axial direction, and harmonic waves satisfy Floquet's theorem of quasi-periodicity on the cell boundary (Brillouin, 1953). Floquet's theorem was first applied to harmonic wave propagation in regular composites by Kohn *et al.* (1972). To date, phase velocity spectra for RC columns have not yet been reported.

The Floquet waves in RC columns exhibit strong dispersion in both longitudinal and flexural modes. It was found that this dispersion in acoustic (lowest) modes was not accurately predicted by the elementary theories. The effect of transverse steel in the form of tie bars on phase velocity spectra of acoustic modes was found negligible due to small volume fractions. In addition, the effects on dispersion of both cross sectional geometry and increasing volume fractions of longitudinal bars were investigated by neglecting the tie bars. The present Floquet wave analyses may be useful for the development of advanced RC beam-column models and nondestructive characterization of RC columns.

FORMULATION OF THE PROBLEM

Harmonic wave propagation in infinitely long RC beam-columns with regular rebar arrangements is considered. The steel reinforcement consists of longitudinal bars and transverse spiral or tie bars. The regularly heterogeneous structure of a RC column is shown with a unit cell in Fig. 1. In the figure, a tied column is shown. However, the subsequent analysis will apply to both tied and spiral columns. Let the x_3-axis be selected in the direction of the column axis, and the x_1,x_2-plane be the cross sectional plane. The x_1, x_2, and x_3 axes form a rectangular Cartesian coordinate system. The region of the unit cell

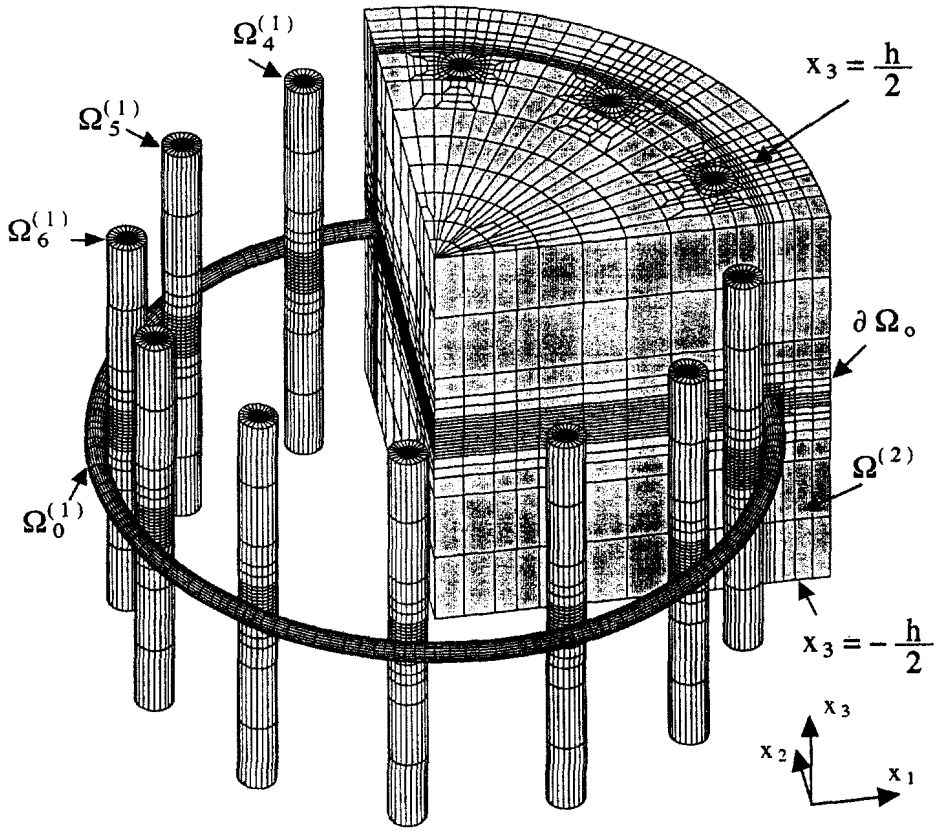

Fig. 2. A finite element mesh and steel reinforcement in the cell.

Ω consists of non-overlapping sub-regions of: concrete, $\Omega^{(2)}$, a tie bar, $\Omega_0^{(1)}$, and the longitudinal bars, $\Omega_m^{(1)}$, $m = 1, 2, \ldots, N$, where N denotes the number of longitudinal bars. Therefore, the cell region is expressed as:

$$\Omega = \Omega^{(1)} \bigcup \Omega^{(2)}, \quad \Omega^{(1)} = \bigcup_{m=0}^{N} \Omega_m^{(1)}, \quad \Omega_m^{(1)} \cap \Omega^{(2)} = \varnothing, \quad \Omega_m^{(1)} \cap \Omega_n^{(1)} = \varnothing \quad \text{if } m \neq n, \tag{1}$$

where $\varnothing$ denotes a null set. For notational simplicity, the superscript (α) denotes variables associated with material $\alpha = 1$ (steel) and 2 (concrete). The steel bar sub-regions, discretized into eight-node hexahedral (brick) elements, are shown in Fig. 2. The boundary of each region is denoted by $\partial\Omega$. Let the length of the cell in the x_3-direction be h and the origin of the coordinate system be placed at the center of the cell. The boundary of the cell, $\partial\Omega$, includes the upper and lower boundary of the cell at $x_3 = \pm h/2$ as well as the lateral surface, $\partial\Omega_o$, whose unit outward normal is denoted by $n_i^{(2)}$.

In what follows, Cartesian indicial notation is employed with the summation convention for repeated indices. Let u_i denote the displacement vector field, and ε_{ij} and σ_{ij} be the symmetric strain and stress tensor fields, respectively. The over-barred quantities denote the values in the time domain. For harmonic motion with angular frequency ω, the displacement vector, strain tensor, and stress tensor fields take the form:

$$[\bar{u}_i\, \bar{\varepsilon}_{ij}\, \bar{\sigma}_{ij}](x_1, x_2, x_3, t) = [u_i\, \varepsilon_{ij}\, \sigma_{ij}](x_1, x_2, x_3, \omega) \exp(-\sqrt{-1}\omega t). \tag{2}$$

where t denotes time, and u_i, ε_{ij}, and σ_{ij} are the complex amplitudes of displacements, strains, and stresses, respectively. The physical components of those variables are the real or imaginary part of the above quantities. For notational simplicity, $\sqrt{(-1)}$ is used, instead of i, to avoid any confusion with the $i(=1, 2, 3)$ used for indicial notation. The harmonic equations of motion are expressed as:

$$\sigma_{ji,j}^{(\alpha)} + \rho^{(\alpha)}\omega^2 u_i^{(\alpha)} = 0 \quad \text{in } \Omega^{(\alpha)}, \tag{3}$$

where $(\,)_{,j} = \partial(\,)/\partial x_j$, and ρ is mass density.

Hooke's law for isotropic steel ($\alpha = 1$) and concrete ($\alpha = 2$) is described as:

$$\begin{aligned}\sigma_{ij}^{(\alpha)} &= C_{ijmn}^{(\alpha)}\varepsilon_{mn}^{(\alpha)} \\ &= \frac{E^{(\alpha)}}{(1+\nu^{(\alpha)})}\left[\frac{\nu^{(\alpha)}}{(1-2\nu^{(\alpha)})}\varepsilon_{kk}^{(\alpha)}\delta_{ij} + \varepsilon_{ij}^{(\alpha)}\right] \quad \text{in } \Omega^{(\alpha)},\end{aligned} \tag{4}$$

where C_{ijmn} is the elastic modulus tensor, E is Young's modulus, ν is Poisson's ratio, and δ_{ij} is the Kronecker delta ($\delta_{ij} = 1$ if $i = j$, $\delta_{ij} = 0$ if $i \neq j$).

The strain-displacement relations are

$$\varepsilon_{mn}^{(\alpha)} = \tfrac{1}{2}(u_{m,n}^{(\alpha)} + u_{n,m}^{(\alpha)}) \quad \text{in } \Omega^{(\alpha)}. \tag{5}$$

The interfacial boundary conditions consist of the continuity of displacements and tractions between each bar and concrete, $\partial\Omega_m^{(1)}$:

$$u_i^{(1)} = u_i^{(2)}, \quad \sigma_{ji}^{(1)}n_j^{(1)} = \sigma_{ji}^{(2)}n_j^{(1)} \quad \text{on } \partial\Omega_m^{(1)}, \quad m = 0, 1, \ldots, N, \tag{6}$$

where $n_j^{(1)}$ is the unit, outward normal to $\Omega_m^{(1)}$.

The boundary conditions on the cell boundary, $\partial\Omega$, consist of the traction-free condition on the lateral surface, $\partial\Omega_o$:

$$\sigma_{ji}^{(2)}n_j^{(2)} = 0 \quad \text{on } \partial\Omega_o, \tag{7}$$

and the Floquet quasi-periodicity conditions on the upper and lower boundary planes, $x_3 = \pm h/2$:

$$u_i^{(\alpha)}\left(x_1, x_2, \frac{h}{2}, \omega\right) = \exp(\sqrt{-1}kh)u_1^{(\alpha)}\left(x_1, x_2, -\frac{h}{2}, \omega\right), \tag{8a}$$

$$\sigma_{3i}^{(\alpha)}\left(x_1, x_2, \frac{h}{2}, \omega\right) = \exp(\sqrt{-1}kh)\sigma_{3i}^{(\alpha)}\left(x_1, x_2, -\frac{h}{2}, \omega\right), \tag{8b}$$

where k is the Floquet wave number which is related to the wavelength Λ as $k = 2\pi/\Lambda$. Due to the quasi-periodicity condition, for a given wave number k, only special angular frequencies (eigenvalues) satisfy the above set of equations (3)–(8). The relationship between k and ω furnishes the dispersion spectra for RC columns.

It is noted that Floquet's theorem has only been applied to a cell with a one dimensional laminated structure. Therefore, the present application of Floquet's theorem to regular RC columns may be equivalent to the use of Bloch's theorem with the wave vector limited to the axial direction. Bloch's theorem has been applied to three dimensional infinite regions with regular microstructure, such as regular crystal lattice structures and composite materials. In Bloch's theorem, the quasi-periodicity conditions are prescribed throughout the outer cell boundary (Brillouin, 1953; Kohn *et al.* 1972).

The above strong formulation for the problem can be cast in a variational form by utilizing Hamilton's principle (Kohn *et al.* 1972):

$$\delta\left[\sum_{\alpha=1}^{2}\iiint_{\Omega^{(\alpha)}}\frac{1}{2}(\rho^{(\alpha)}\omega^2 u_i^{(\alpha)}u_i^{(\alpha)*}-C_{ijmn}^{(\alpha)}\varepsilon_{ij}^{(\alpha)}\varepsilon_{mn}^{(\alpha)*})\,dx_1\,dx_2\,dx_3\right]=0, \tag{9}$$

where $\delta(\,)$ implies the variation of $(\,)$, and $(\,)^*$ indicates the complex conjugate of $(\,)$. The above equation yields

$$\sum_{\alpha=1}^{2}\iiint_{\Omega^{(\alpha)}}(-\delta\varepsilon_{ij}^{(\alpha)*}\sigma_{ij}^{(\alpha)}+\delta u_i^{(\alpha)*}\rho^{(\alpha)}\omega^2 u_i^{(\alpha)}+c.c.)\,dx_1\,dx_2\,dx_3=0, \tag{10}$$

where "*c.c.*" denotes the complex conjugate of the preceding terms.

Admissible displacements are continuous up to the second spatial derivatives in each sub-region and satisfy (6a) and (8a). Since Hamilton's principle is a displacement-based variational formulation, eqns (4) and (5) become definitions or constraints. For admissible displacement fields, the Euler-Lagrange equations of (10) yield the equations of motion, (3), the interfacial traction continuity, (6b), the traction free condition on the lateral cell boundary, (7), and the quasi-periodicity condition for the traction (8b).

In order to solve the above problem, the displacement and stress fields are expressed in the form:

$$u_i^{(\alpha)}(x_1,x_2,x_3,\omega)=\tilde{u}_i^{(\alpha)}(x_1,x_2,x_3,\omega;k)\exp(\sqrt{-1}kx_3), \tag{11a}$$

$$\sigma_{ij}^{(\alpha)}(x_1,x_2,x_3,\omega)=\tilde{\sigma}_{ij}^{(\alpha)}(x_1,x_2,x_3,\omega;k)\exp(\sqrt{-1}kx_3). \tag{11b}$$

By virtue of the quasi-periodicity conditions, (8), the tilded quantities satisfy the periodicity conditions:

$$\tilde{u}_i^{(\alpha)}\left(x_1,x_2,\frac{h}{2},\omega;k\right)=\tilde{u}_i^{(\alpha)}\left(x_1,x_2,-\frac{h}{2},\omega;k\right), \tag{12a}$$

$$\tilde{\sigma}_{3i}^{(\alpha)}\left(x_1,x_2,\frac{h}{2},\omega;k\right)=\tilde{\sigma}_{3i}^{(\alpha)}\left(x_1,x_2,-\frac{h}{2},\omega;k\right). \tag{12b}$$

In order to solve the Floquet wave problem, a semi-analytical finite element procedure was utilized by extending the scheme developed by Murakami and Akiyama (1985) for the Floquet wave analyses in regularly laminated composites.

SEMI-ANALYTICAL FINITE ELEMENT ANALYSES

A cell region is discretized into eight-node brick elements. The mesh used for the numerical analyses is shown in Fig. 2. The long cylinders represent the steel sub-regions. In order to take advantage of the symmetry and antisymmetry conditions, only one quadrant of the cell was discretized. The mesh contains 20,705 nodes and 20,520 brick elements. Each node has three translational degrees-of-freedom in complex form. Finite element regions are denoted by $\Gamma^{(e)}$, $e=1,2,\ldots,N_{el}$:

$$\Omega=\bigcup_{e=1}^{N_{el}}\Gamma^{(e)},\quad \Gamma^{(e)}\bigcap\Gamma^{(f)}=\varnothing\quad \text{if } e\neq f, \tag{13}$$

where N_{el} is the total number of brick elements.

In a typical isoparameteric element, $\Gamma^{(e)}$, the complex displacement field is approximated by nodal displacements (for example, Hughes, 1987):

$$\{u\}^{(e)} = [N]^{(e)}\{\tilde{U}\}^{(e)} \exp(\sqrt{-1}kx_3) \quad \text{in } \Gamma^{(e)}, \tag{14a}$$

in which $\{u\}$ is the 3×1 displacement matrix:

$$\{u\}^{(e)} = [u_1^{(e)}\ u_2^{(e)}\ u_3^{(e)}]^{\mathrm{T}}, \tag{14b}$$

where $[]^{\mathrm{T}}$ denotes the transpose of $[]$. In addition, $[N]$ is the 3×24 interpolation matrix, and $\{\tilde{U}\}$ represents the complex 24×1 nodal displacement matrix. These matrices are defined in Appendix A.

By utilizing (14) in (5), the strain-nodal displacement relation becomes

$$\{\varepsilon\}^{(e)} = [B]^{(e)}\{\tilde{U}\}^{(e)} \exp(\sqrt{-1}kx_3) \quad \text{in } \Gamma^{(e)}, \tag{15a}$$

where $\{\varepsilon\}$ is the 6×1 strain matrix,

$$\{\varepsilon\}^{(e)} = [\varepsilon_{11}^{(e)}\ \varepsilon_{22}^{(e)}\ \varepsilon_{33}^{(e)}\ 2\varepsilon_{23}^{(e)}\ 2\varepsilon_{31}^{(e)}\ 2\varepsilon_{12}^{(e)}]^{\mathrm{T}}, \tag{15b}$$

and $[B]$ is the complex 6×24 strain-displacement matrix, defined in Appendix A.

Hooke's law (4) is rewritten in matrix form as:

$$\{\sigma\}^{(e)} = [D]^{(e)}\{\varepsilon\}^{(e)} \quad \text{in } \Gamma^{(e)}, \tag{16a}$$

where $\{\sigma\}$ is the 6×1 stress matrix,

$$\{\sigma\}^{(e)} = [\sigma_{11}^{(e)}\sigma_{22}^{(e)}\sigma_{33}^{(e)}\sigma_{23}^{(e)}\sigma_{31}^{(e)}\sigma_{12}^{(e)}]^{\mathrm{T}}, \tag{16b}$$

and $[D]$ is the 6×6 elastic modulus matrix, defined in Appendix A. The matrix $[D]$ is constructed by utilizing the appropriate elastic moduli of material α $(= 1, 2)$.

The substitution of (14)–(16) into (10) yields

$$\sum_{e=1}^{N_{el}} \iiint_{\Gamma^{(e)}} (-\delta\{\varepsilon^*\}^{(e)T}\{\sigma\}^{(e)} + \omega^2 \delta\{u^*\}^{(e)T}\rho^{(e)}\{u\}^{(e)})\, \mathrm{d}x_1\, \mathrm{d}x_2\, \mathrm{d}x_3 + c.c.$$

$$= \sum_{e=1}^{N_{el}} \delta\{\tilde{U}^*\}^{(e)T}(-[K]^{(e)}\{\tilde{U}\}^{(e)} + \omega^2[M]^{(e)}\{\tilde{U}\}^{(e)}) + c.c. = 0, \tag{17}$$

where $[K]^{(e)}$ is the element stiffness matrix, which is a 24×24 Hermitian matrix,

$$[K]^{(e)} = \iiint_{\Gamma^{(e)}} [B^*]^{(e)T}[D]^{(e)}[B]^{(e)}\, \mathrm{d}x_1\, \mathrm{d}x_2\, \mathrm{d}x_3, \tag{18a}$$

and $[M]^{(e)}$ is the element mass matrix, which is a 24×24 (real) symmetric matrix,

$$[M]^{(e)} = \iiint_{\Gamma^{(e)}} [N]^{(e)T}\rho^{(e)}[N]^{(e)}\, \mathrm{d}x_1\, \mathrm{d}x_2\, \mathrm{d}x_3. \tag{18b}$$

In (17) the following complex conjugates of the variations of (14a) and (15a) have been utilized:

$$\delta\{u^*\}^{(e)T} = \delta\{\tilde{U}^*\}^{(e)T}[N]^{(e)T} \exp(-\sqrt{-1}kx_3), \tag{19a}$$

$$\delta\{\varepsilon^*\}^{(e)T} = \delta\{\tilde{U}^*\}^{(e)T}[B^*]^{(e)T} \exp(-\sqrt{-1}kx_3). \tag{19b}$$

Assembling both element stiffness and mass matrices for the global degrees-of-freedom, the Euler-Lagrange equations of (17) yield an algebraic eigenvalue problem,

$$[K]\{\tilde{U}\} = \omega^2[M]\{\tilde{U}\}. \tag{20}$$

In (20), the global stiffness matrix $[K]$ is Hermitian, $[K]^{*\mathrm{T}} = [K]$, and the global mass matrix $[M]$ is real and symmetric, $[M]^{\mathrm{T}} = [M]$. The lumped mass matrix was constructed by employing the row-sum algorithm (Hughes, 1987, Chapter 7).

For a given wave number k, (20) is numerically solved for eigenvalues, ω^2, and corresponding eigenvectors, $\{\tilde{U}\}$, by employing the inverse iteration method. It is known that Hermitian matrices have all real eigenvalues (Noble and Daniel, 1977). Phase velocity C_p and group velocity C_g are obtained as:

$$C_p = \frac{\omega}{k}, \quad C_g = \frac{\mathrm{d}\omega}{\mathrm{d}k}. \tag{21}$$

In the numerical analyses, it is convenient to nondimensionalize Young's modulus and mass density by those of concrete. Spatial variables, displacements, and the cell length, h, are nondimensionalized by a reference cross-sectional diameter d. With this nondimensionalization, wave number $kd = 2\pi d/\Lambda$, is prescribed and the eigenvalue problem, (20), is numerically solved for eigenpairs starting from the lowest modes,

$$\left(\frac{\omega_\beta d}{C_0}, \frac{1}{d}\{\tilde{U}\}_\beta\right), \quad \beta = 1, 2, \ldots \tag{22}$$

where $C_0 = \sqrt{(E^{(2)}/\rho^{(2)})}$ is the concrete bar velocity.

The above eigenvalue analyses were conducted by using the CRAY C90 at the San Diego Supercomputer Center. The global stiffness matrix was stored in skyline format (Hughes, 1987, Chapter 11). The first lowest 15 modes were computed by using the inverse iteration method with the shifting to higher modes (Hughes, 1987, Chapter 10). The existing triangularization algorithm for real symmetric matrices in skyline storage was generalized for Hermitian matrices. Due to an extremely large requirement for core memory, an out-of-core, skyline triangularization scheme for Hermitian matrices was implemented upon column partitioning.

In order to assess the accuracy of elementary theories in predicting harmonic wave propagation, phase velocities of the elementary theories were derived in Appendix B.

NUMERICAL RESULTS

Phase velocity spectra and corresponding mode shapes were computed for the RC column with circular cross section of diameter, $d = 500$ mm and cell height, $h = 200$ mm. Twelve vertical steel bars of diameter 25 mm were arranged periodically on the radius 192.5 mm every 30° and a transverse tie bar of diameter 13 mm surrounding the vertical bars was located at a height of 100 mm (shown in Fig. 2). The volume fraction of the vertical rebars is 3%. To incorporate the symmetry and antisymmetry conditions on the x_2, x_3- and x_3, x_1-planes, only the first quadrant of the cell in the $x_1(\geqslant 0)$, $x_2(\geqslant 0)$, x_3-space was discretized into eight-node brick elements. For longitudinal wave motion, the following symmetry conditions were imposed on both the x_2,x_3-plane and the x_1,x_3-plane,

$$\begin{aligned} u_1 = \sigma_{12} = \sigma_{13} = 0 \quad &\text{on } x_1 = 0, \\ u_2 = \sigma_{21} = \sigma_{23} = 0 \quad &\text{on } x_2 = 0. \end{aligned} \tag{23}$$

For flexural wave motion, the symmetry condition on the x_2,x_3-plane and the anti-symmetry condition on the x_1,x_3-plane were imposed,

Table 1. Material properties

	Steel (1)	Concrete (2)
E	210 GPa	21 GPa
ν	0.3	0.15
ρ	7800 kg/m^3	2300 kg/m^3

$$u_1 = \sigma_{12} = \sigma_{13} = 0 \quad \text{on } x_1 = 0,$$
$$u_1 = \sigma_{22} = u_3 = 0 \quad \text{on } x_2 = 0. \tag{24}$$

Material properties employed for the calculations are shown in Table 1.

In the numerical analyses, the phase velocity spectra were computed for the wave number range, $d/\Lambda(= kd/2\pi) = 0$ to 1.2. In order to characterize modes, it is convenient to introduce the displacement field of a wave propagating in a homogeneous cylinder with a circular cross section, which is expressed in cylindrical coordinates, r and θ, as (for example, Graff, 1975):

$$u_r(r,\theta,x_3) = U_r(r)\cos(n\theta-\phi)\exp(\sqrt{-1}kx_3),$$
$$u_\theta(r,\theta,x_3) = U_\theta(r)\sin(n\theta-\phi)\exp(\sqrt{-1}kx_3),$$
$$u_z(r,\theta,x_3) = U_z(r)\cos(n\theta-\phi)\exp(\sqrt{-1}kx_3), \tag{25}$$

where n is an integer and ϕ is real. Having an even number for n with $\phi = 0$ expresses the modes with two planes of symmetry, while an odd number with $\phi = \pi/2$ describes the modes which have planes of both symmetry and anti-symmetry. (An even value for n with $\phi = \pi/2$ exhibits the modes with two planes of anti-symmetry on x_1-x_3 and x_2-x_3 planes.) In the sequel, modes of RC columns are distinguished by using values for n which describe the circumferential modes in a homogeneous circular cylinder. The acoustic modes of $n = 0$ and $n = 1$ represent, respectively, a longitudinal wave and a flexural wave. The propagation of these waves is investigated in RC structural analyses by utilizing elementary rod and beam equations.

Figure 3a shows the dispersion relation (for longitudinal waves) of nondimensional frequency, (22), as a function of d/Λ where d is the diameter of the column and Λ is the wavelength. The dispersion relation is re-plotted in Fig. 3b in terms of phase velocity, defined in (21a), as a function of d/Λ. In the figures, the modes corresponding to the higher circumferential modes, $n = 2$, 4, are also shown in addition to the axisymmetric modes, $n = 0$, in (25). These higher modes propagate at smaller wave velocities than the concrete bar velocity at larger wave numbers. It is noted that the negative slope in the dispersion spectra, in Fig. 3a, implies negative group velocity according to (21b). The branches with negative group velocity near the cutoff have been experimentally observed by Meitzler (1965). In Fig. 3b, the first mode exhibits typical reduction of the phase velocity versus wave number, as observed in the Pochhammer-Chree problem (Onoe *et al.* 1962). At the long wavelength limit ($d/\Lambda \to 0$) the phase velocity is approximately 9% larger than the bar velocity, C_0, of the pure concrete column due to longitudinal steel bars which have 72% larger bar velocity than concrete.

The phase velocity predicted by the elementary rod theory, summarized in Appendix B, is shown in Fig. 3b by straight dashed-lines. The existing FE models are based upon the elementary rod theory, which is nondispersive, as shown in Fig. 3b. The Love-Rayleigh theory incorporates the dispersion in the acoustic (lowest) longitudinal mode induced by the Poisson effect (Fung, 1965, Chapter 11).

The mode shapes corresponding to the longitudinal modes at $d/\Lambda = 0.796$ are shown in Figs. 4a–c. At $d/\Lambda = 0.796$, the first two lowest modes in ascending order are shown in Figs 4a and 4b. These modes are characterized by the circumferential mode number, defined

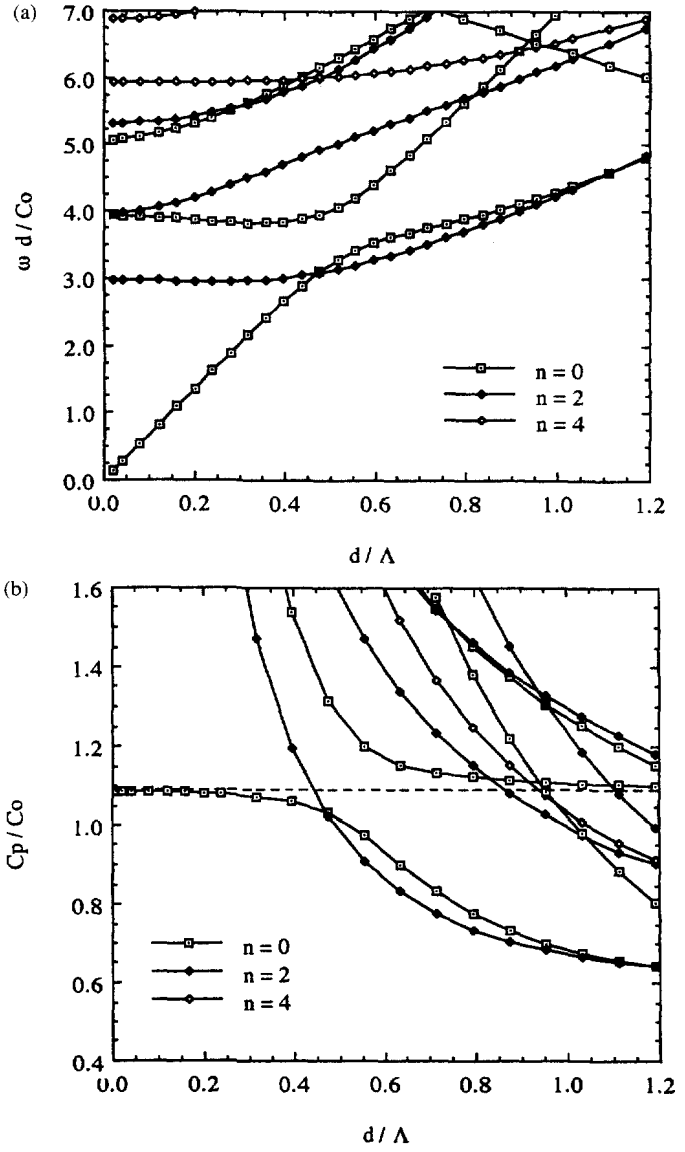

Fig. 3. (a) Dispersion spectra of longitudinal modes. (b) Phase velocity spectra of longitudinal modes.

in (25), $n = 2$ and 0, respectively. Figure 4c illustrates the sixth mode, from the lowest, which first exhibits the effect of the tie bar located at $x_3 = 0$. The mode shape of the axisymmetric mode, $n = 0$, in Fig. 4b, shows the warping of the plane normal to the x_3 axis. This warping function is approximated by a quadratic function of the radial coordinate from the axis.

Figures 5a and 5b show, respectively, the dispersion spectra of frequency and phase velocity with respect to d/Λ. For flexural modes, the first mode exhibits an increasing phase velocity with d/Λ, observed in the Pochhammer and Chree solution for the acoustic flexural mode (Pao and Mindlin, 1960). The phase velocity converges to the surface wave velocity of the column at the short wavelength limit, $d/\Lambda \to \infty$. In addition to the lowest family of flexural modes, $n = 1$, the higher-order circumferential modes, $n = 3$, are also shown. Unstable modes with negative group velocity are observed in Fig. 5a. In Fig. 5b, the phase velocity predicted by the elementary beam theories, derived in Appendix B, are also shown. The Euler-Bernoulli beam theory, shown in Fig. 5b by a dashed line, exhibits a straight spectrum and does not possess a bounding wave speed at the short wavelength limit. The Rayleigh beam theory includes the rotatory inertia effect, which is neglected in the Euler-Bernoulli beam theory. The resulting phase velocity spectra of Rayleigh are shown in Fig.

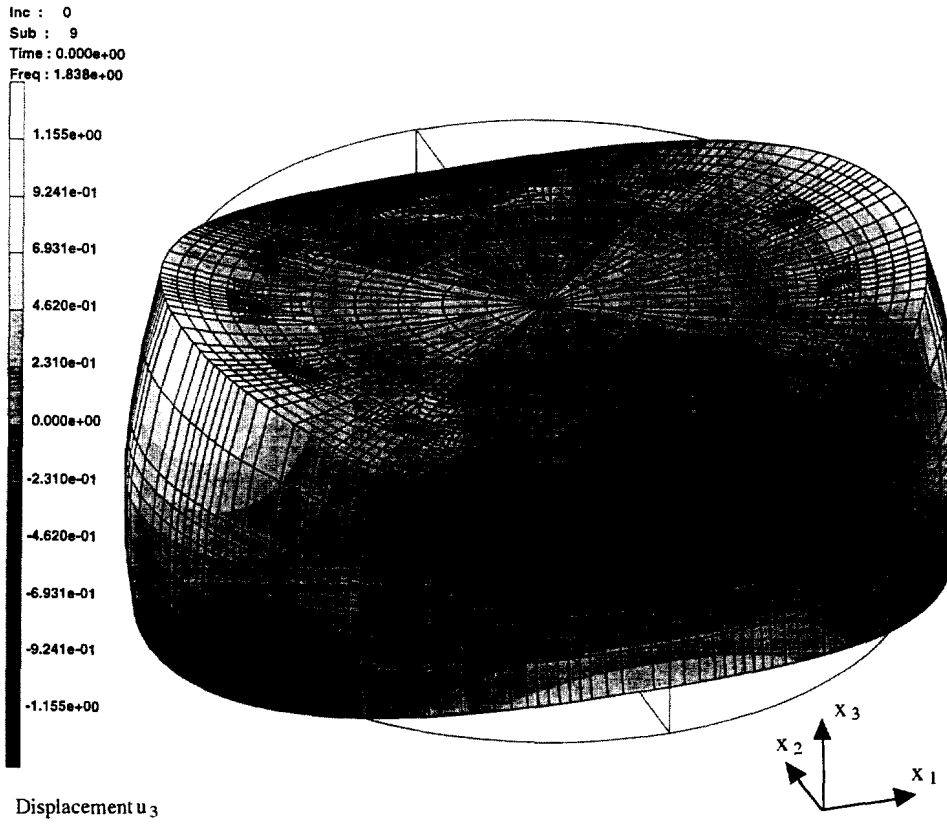

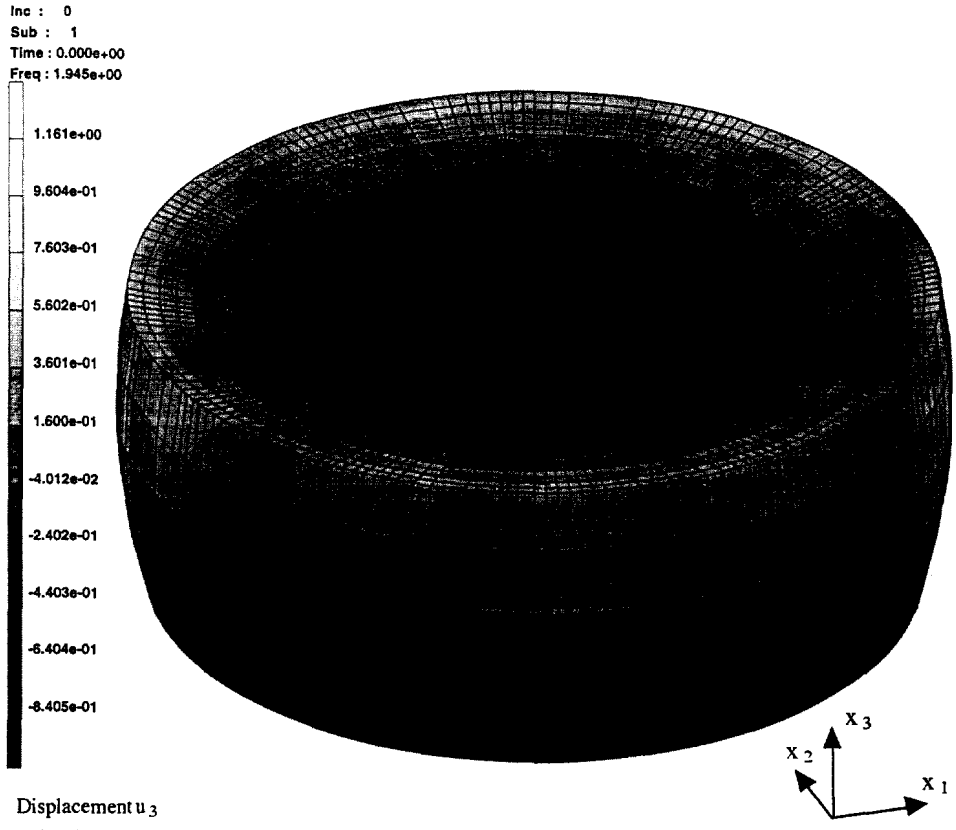

Fig. 4. (a) The lowest mode shape of longitudinal wave motion. (b) The second mode shape of longitudinal wave motion. (c) The sixth mode shape of longitudinal wave motion.

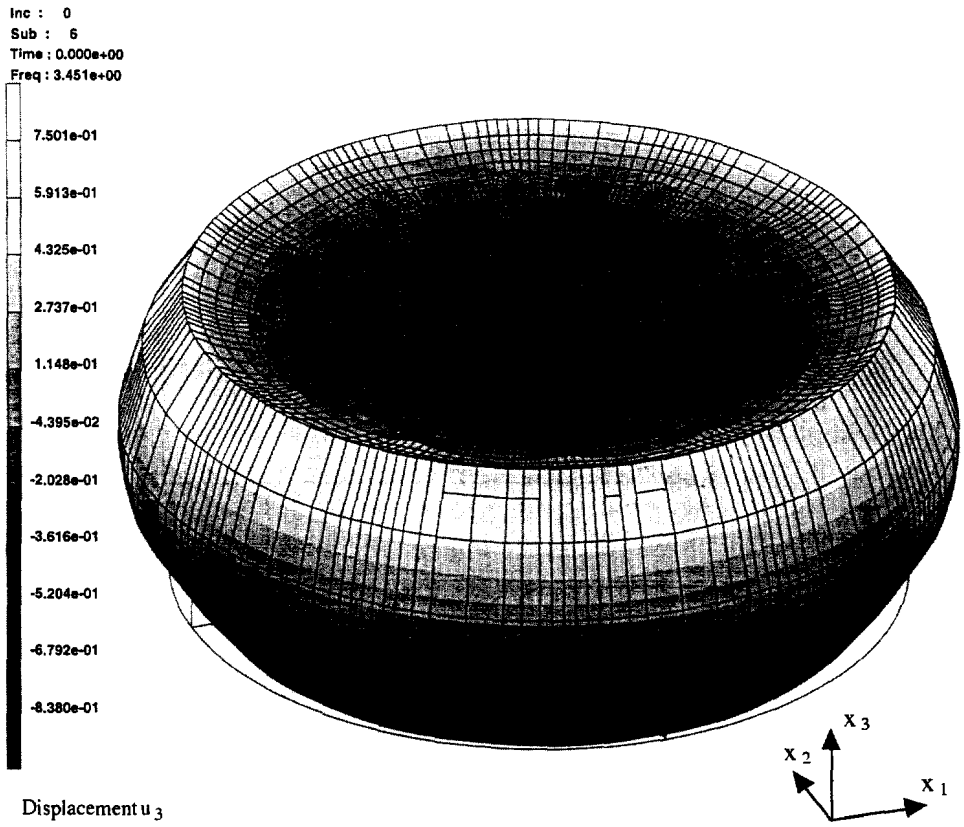

Fig. 4. (c).

5b by a short-dotted line. At the short wave length limit, the Rayleigh beam theory predicts a wave velocity much larger than the correct surface wave velocity. It is known that the effect of transverse shear deformation incorporated in the Timoshenko beam theory, with an appropriate shear correction factor, reduces the limiting wave velocity to the surface wave velocity at the short wave length limit (Mindlin and Herrmann, 1951).

Figures 6a and 6b show the mode shapes of the first two flexural modes at $d/\Lambda = 0.955$ in ascending order. The mode shape of the lowest mode in Fig. 6a is characterized by $n = 1$ and endorses the assumption employed by the beam theories that a plane normal to the beam axis remains plane during flexural deformation. Figure 6b denotes the first optical model of $n = 1$. The fourth mode from the lowest, illustrated in Fig. 6c, exhibits the tie bar effect.

The above comparisons of phase velocity spectra attest that the strong dispersion in acoustic (lowest) modes was not accurately predicted by the elementary theories. In the rod and beam theories, it is assumed that the plane sections normal to the beam axis remain plane during the deformation. Close examinations of the corresponding mode shapes in the acoustic modes, shown in Figs 4 and 6, revealed that the mode shapes can be closely approximated by planes except for the minor "warping" which exists even at the long wavelength limit, $d/\Lambda \to 0$. For flexural wave motion, the high-order RC beam models which neglect minor warping can accurately predict wave dispersion. However, for longitudinal wave motion, the warping of the plane section normal to the column axis must be incorporated into RC rod models (Murakami and Yamakawa, 1997).

In the next section, the effect of the tie bars on the acoustic longitudinal and flexural modes are investigated.

WAVEGUIDE APPROXIMATION

To assess the effect of tie bars on the dispersion of acoustic longitudinal and flexural modes, phase velocity analyses were conducted by neglecting tie bars. The quasi-periodicity

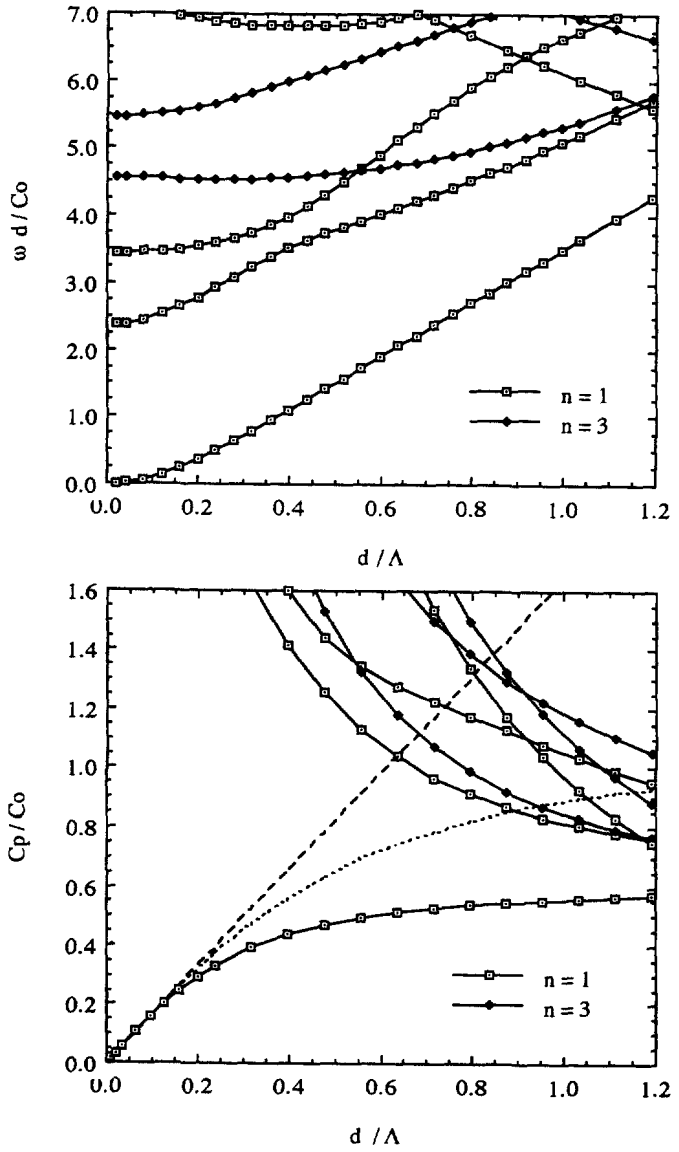

Fig. 5. (a) Dispersion spectra of flexural modes. (b) Phase velocity spectra of flexural modes.

conditions, (8), are no longer required. The displacement and stress fields are expressed in the form:

$$u_i^{(\alpha)}(x_1, x_2, x_3, \omega) = \tilde{u}_i^{(\alpha)}(x_1, x_2, k, \omega) \exp(\sqrt{-1} k x_3), \tag{26a}$$

$$\sigma_{ij}^{(\alpha)}(x_1, x_2, x_3, \omega) = \tilde{\sigma}_{ij}^{(\alpha)}(x_1, x_2, k, \omega) \exp(\sqrt{-1} k x_3). \tag{26b}$$

The tilded quantities are independent of the x_3-coordinate. Therefore, the problem reduces to a two-dimensional waveguide analysis. The variational equation, (10), is also used for this case by performing integration over a unit length in x_3, since the integrands are independent of x_3. The cross sectional region on $x_3 = h/2$ is now discretized into four-node quadrilateral elements. Necessary changes associated with the two dimensional elements can be easily made in $[N]$ and $[B]$. After assembling for global degrees-of-freedom, the same eigenvalue problem as (20) is obtained. The phase velocity spectra, obtained by neglecting tie bars (using the waveguide approximation), are shown in Fig. 7a for longitudinal modes and in Fig. 7b for flexural modes. In these figures, the phase velocity spectra for RC columns without tie bars are shown in solid lines overlaid with the spectra of the Floquet waves in dashed lines. The latter lines were already shown in Figs 3b and 5b, respectively. The

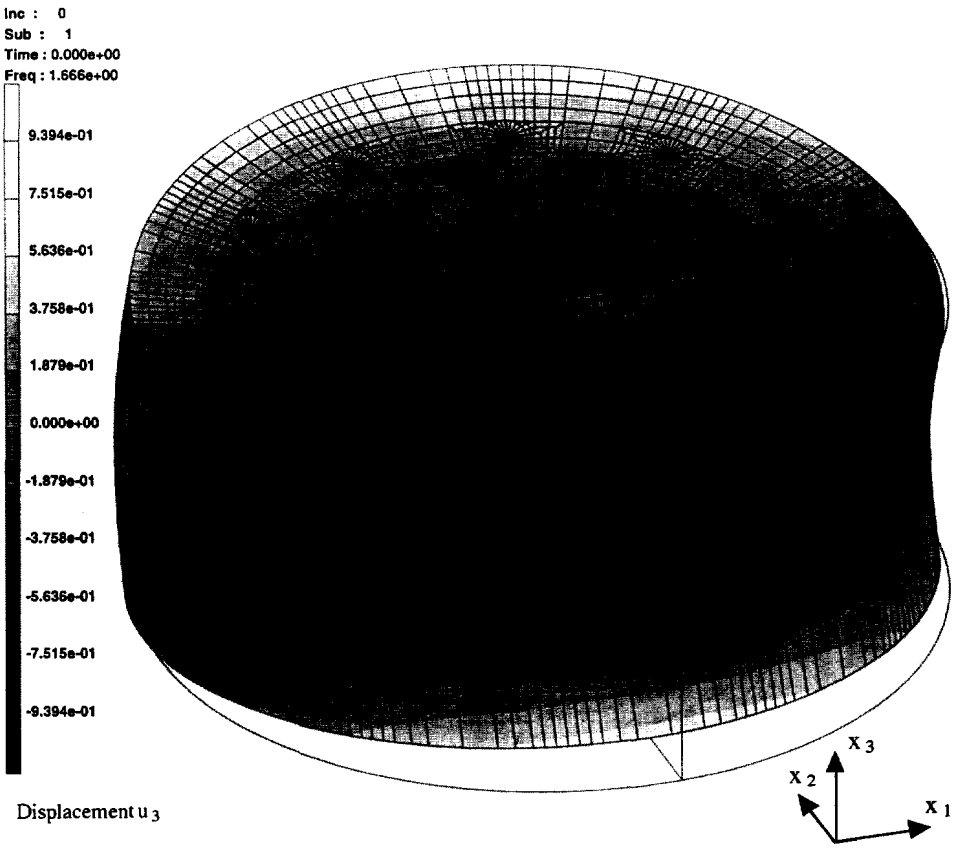

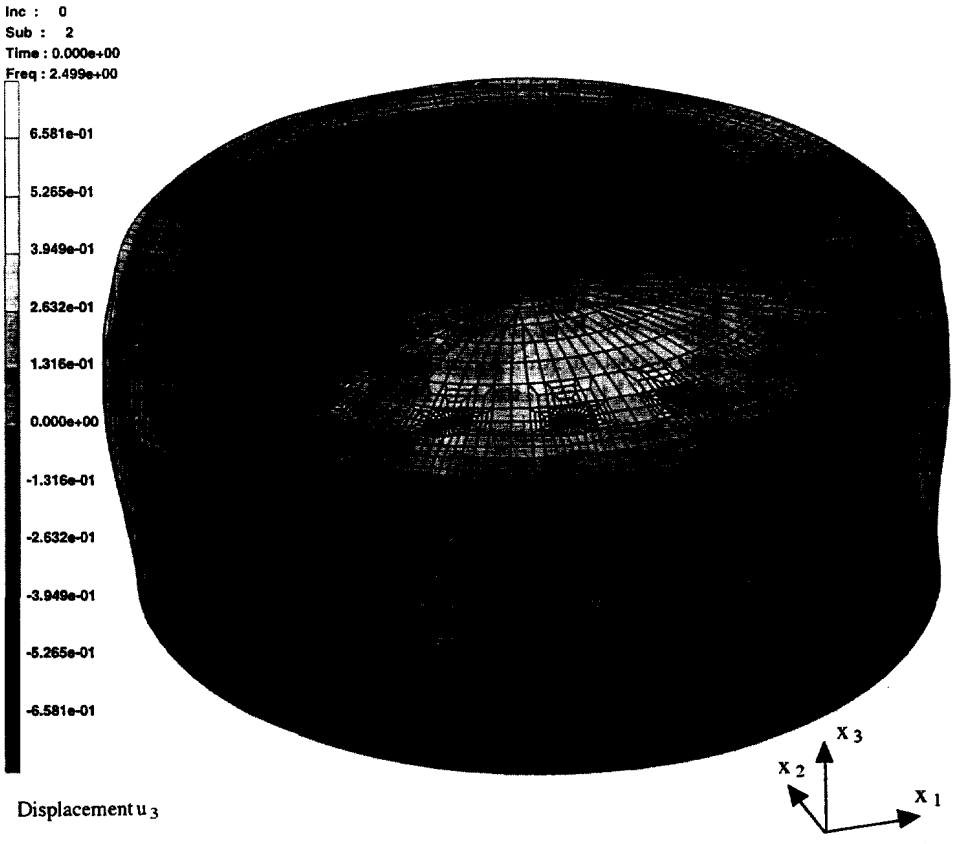

Fig. 6. (a) The lowest mode shape of flexural wave motion. (b) The second mode shape of flexural wave motion. (c) The fourth mode shape of flexural wave motion.

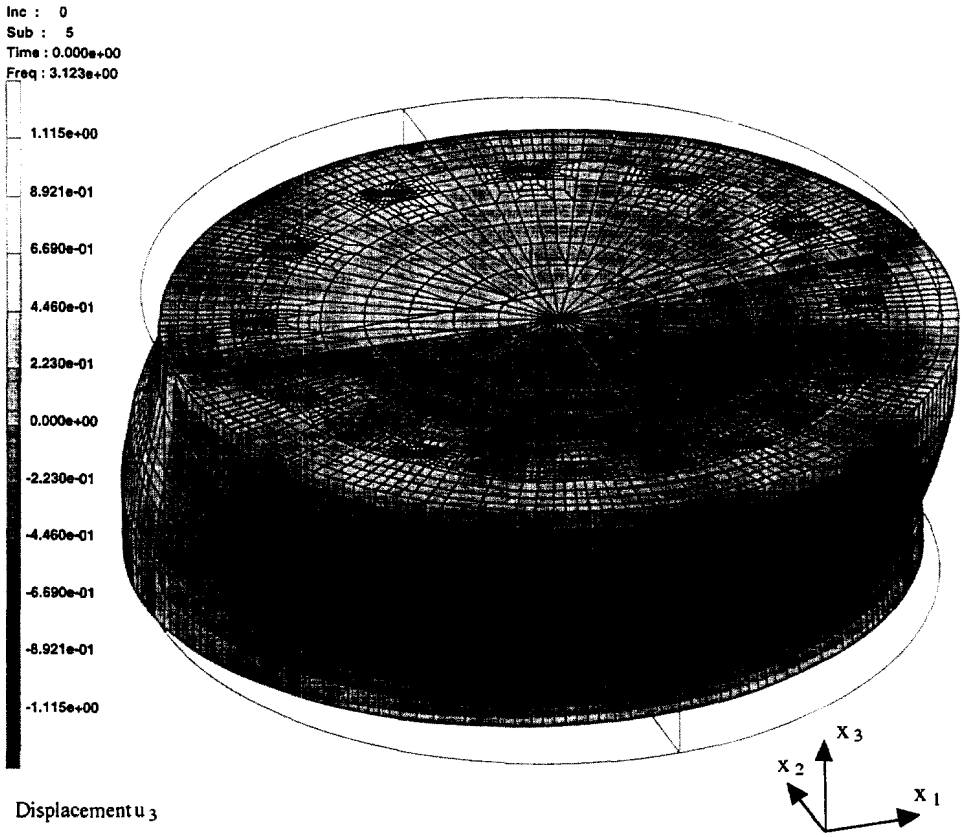

Fig. 6. (c).

waveguide analysis successfully captured most modes except the higher modes, shown by dashed lines, with negative group velocity. Figure 7 clearly shows that for $h/d = 0.4$ tie bars may be neglected in the wave propagation of acoustic modes. For several wave numbers, the Floquet wave analyses were conducted for $h/d = 0.2$ and 1.0 to investigate the effect of tie-bars. It was found that the tie-bar effect is negligible for small $h/d(< 0.4)$. However, for larger h/d, tie-bar modes appear as shear modes in the low wave number range. It is noted that newly built RC columns will have smaller h/d. For example, after the Tokachi-oki earthquake in 1968, which caused a substantial number of columns to fail in shear, the Japanese code was revised in 1971 to limit the maximum spacing of transverse reinforcement to 10 cm at the ends of the columns and 15 cm elsewhere (Architectural Institute of Japan, 1995).

By utilizing the economical waveguide approximation, the effect of cross sectional geometry was investigated. The square and octagonal cross sections of RC columns, shown in Fig. 8, have the same cross-sectional area as the column, shown in Fig. 1, with the same longitudinal bars. The resulting phase velocity spectra are shown in Figs 9a and 10a for longitudinal modes and in Figs 9b and 10b for flexural modes for square and octagonal cross sections, respectively. In Figs 9 and 10, the phase velocity spectra for a circular cross section are also plotted by dashed lines. These figures indicate that the details of the cross sectional geometry does not significantly alter the dispersion of the acoustic modes, as long as the steel volume fraction is identical. However, the phase velocity of higher modes for a square cross section clearly show the difference in the dispersion spectra compared to those of the circular cross section.

To investigate the effect of increasing vertical bars on dispersion of acoustic modes, the phase velocity spectra were computed for the column in Fig. 1 by changing the number of longitudinal bars from twelve to eight and twenty. The results are shown in Fig. 11a for longitudinal modes and in Fig. 11b for flexural modes. It is seen that changing the steel

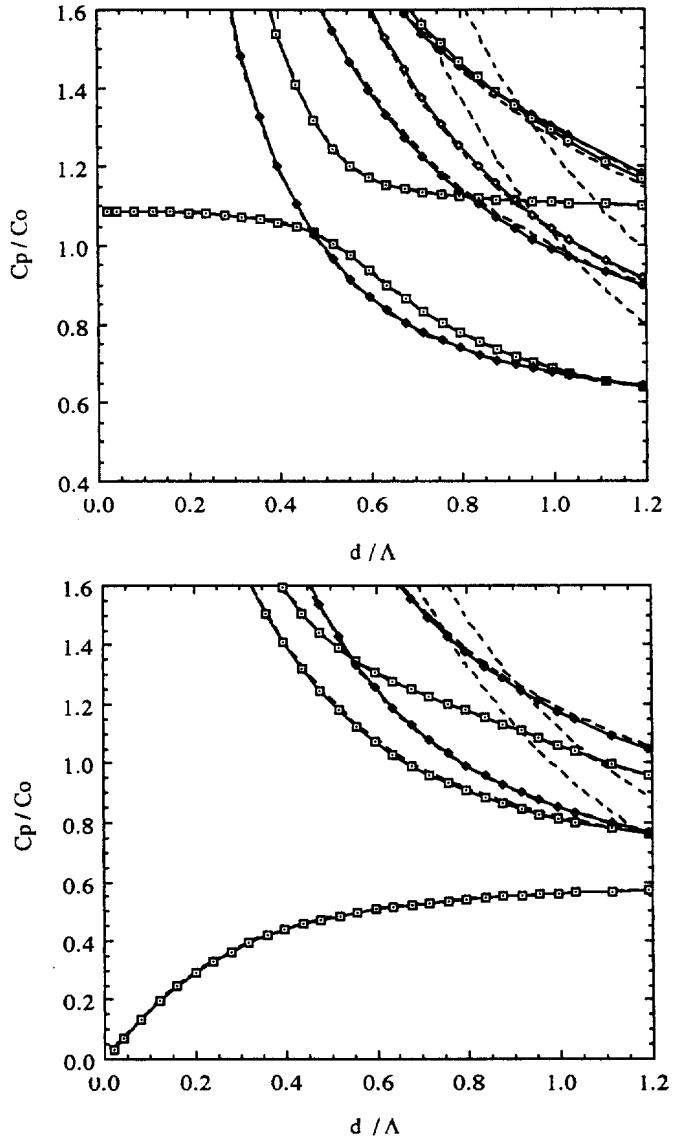

Fig. 7. (a) Waveguide approximation for phase velocity spectra of longitudinal modes. (b) Waveguide approximation for phase velocity spectra of flexural modes.

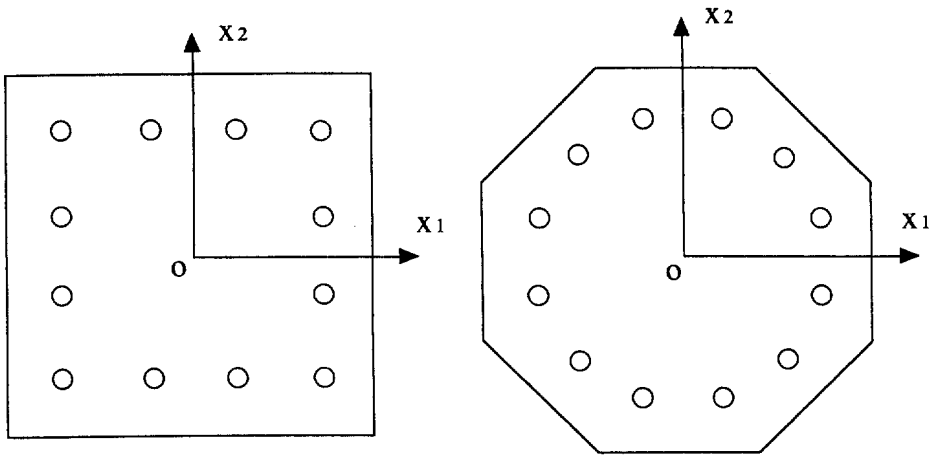

Fig. 8. RC columns with square and octagonal cross sections.

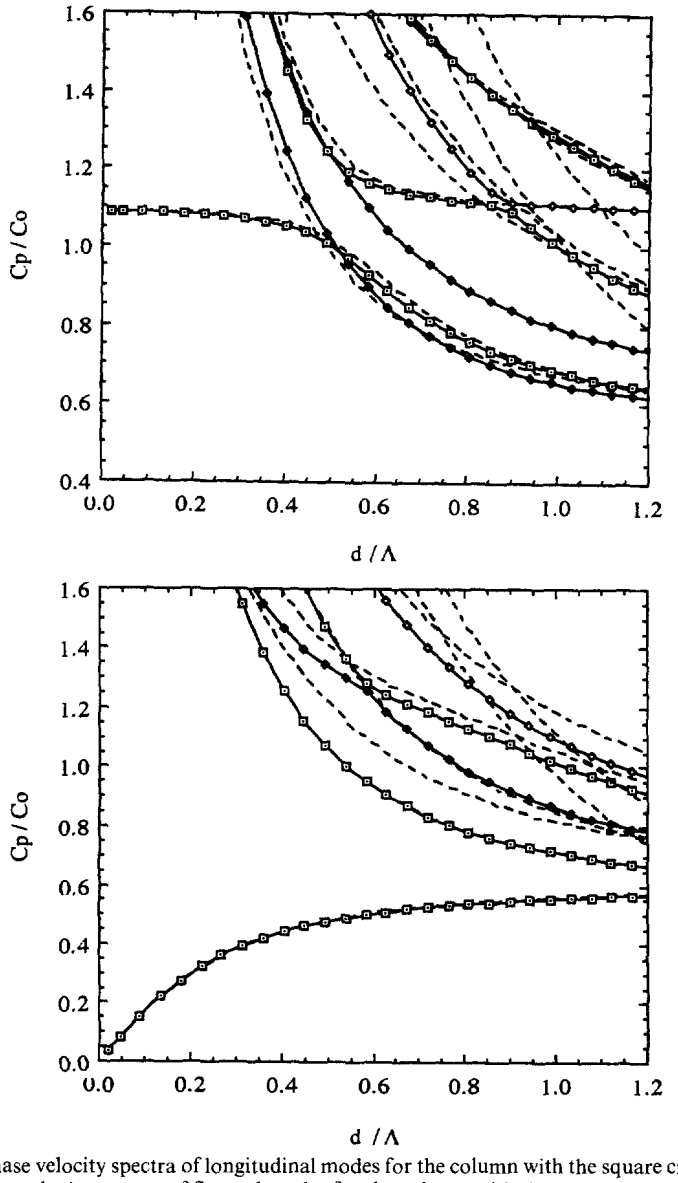

Fig. 9. (a) Phase velocity spectra of longitudinal modes for the column with the square cross section. (b) Phase velocity spectra of flexural modes for the column with the square cross section.

volume fraction exhibits marked effect in the dispersion of the acoustic longitudinal mode, while change in the steel volume fraction induces moderate changes in flexural modes. The bar velocity change in Fig. 11a at the long wavelength limit can be accurately predicted by the elementary rod theory in Appendix B.

CONCLUSIONS

In order to assess the accuracy of elementary rod and beam theories employed in finite element structural analyses for propagating elastic waves in RC beam-columns, Floquet wave analyses were conducted to obtain longitudinal and flexural phase velocity spectra. The spectra exhibit strong dispersion similar to the Pochhammer and Chree problem of homogeneous circular cylinders. The comparisons of the spectra with those predicted by the elementary theories revealed that the dispersion in acoustic (lowest) modes was not accurately predicted by the elementary theories. However, it was found that the acoustic mode shapes of the Floquet waves can be closely approximated by plane sections. This

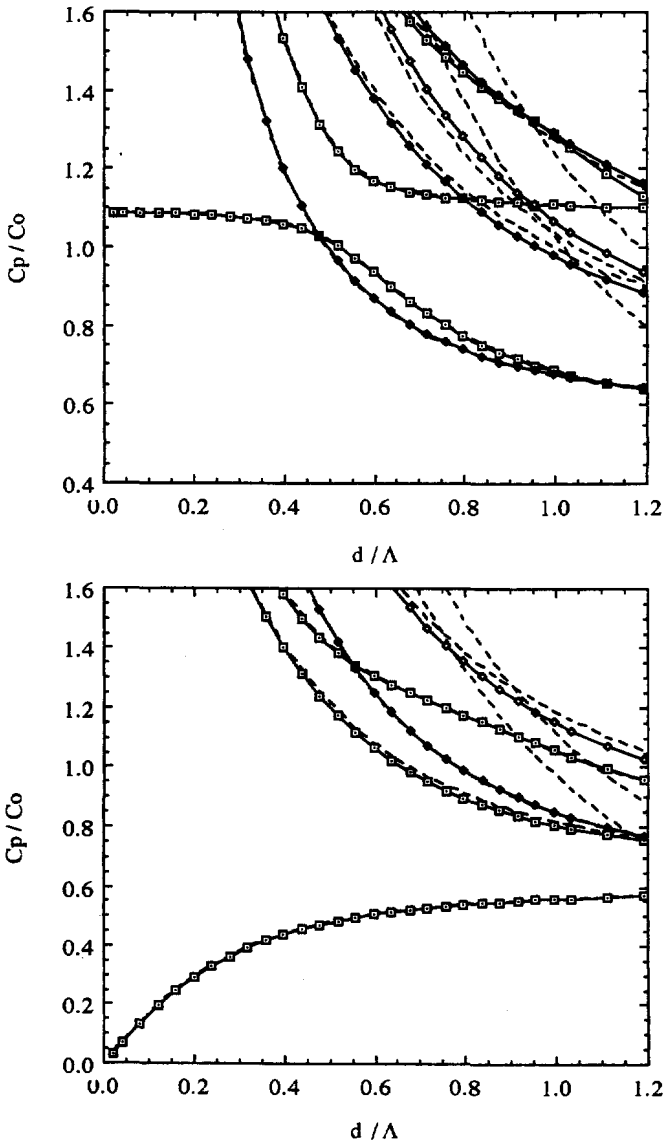

Fig. 10. (a) Phase velocity spectra of longitudinal modes for the column with the octagonal cross section. (b) Phase velocity spectra of flexural modes for the column with the octagonal cross section.

observation is consistent with the assumptions of elementary rod and beam theories. The effect of tie-bars can be ignored for wave propagation analyses of RC columns with small spacing of transverse reinforcement, $h/d < 0.4$. For equal volume fraction of vertical rebars, the effect of cross sectional geometry on dispersion of acoustic longitudinal and flexural modes was negligible, justifying the use of elementary rod and beam models for structural analyses. The increase or reduction of vertical bars significantly alters the bar velocity of the column, thus changing the dispersion of the acoustic longitudinal mode. The change in the acoustic flexural mode due to the changing volume fraction of vertical rebars was negligible.

Acknowledgement—The authors are thankful to Dr Thomas J. Impelluso at University of California, San Diego (UCSD) for his advise on subdomain analyses and vectorizing the finite element code. The finite element calculation was performed by utilizing the CRAY C90 at the San Diego Supercomputer Center through the UCSD Block Grant Allocation. A pre- and post-processor, MENTAT, developed by MARC Analysis Research Corporation was utilized for mesh generation and post processing—the authors are thankful to Mr Reza Sadeghi for his software support.

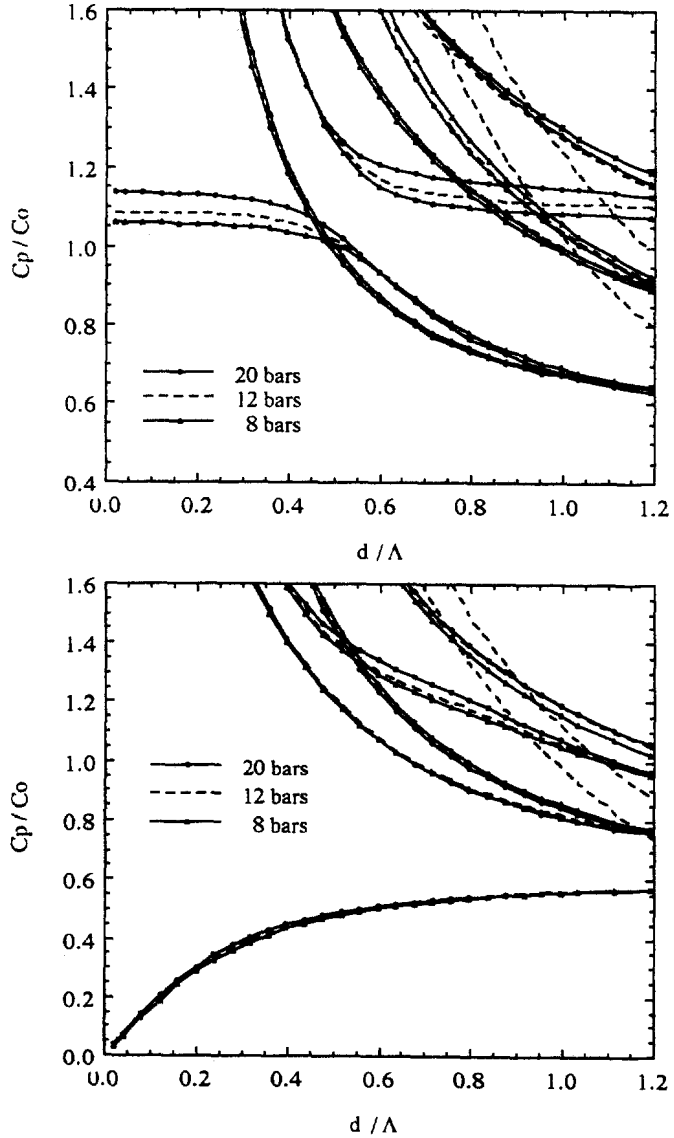

Fig. 11. (a) Phase velocity spectra of longitudinal modes for the circular columns with 8, 12, and 20 vertical bars. (b) Phase velocity spectra of flexural modes for the circular columns with 8, 12, 20 vertical bars.

REFERENCES

Architectural Institute of Japan (1995) *Preliminary Reconnaissance Report of the* 1995 *Hyogoken-Nanbu Earthquake*, English Edition. Tokyo, Japan.

Armenakas, A. E. (1970) Propagation of harmonic waves in composite circular cylindrical rods. *Journal of the Acoustical Society of America*, **47**, 822–837.

Brillouin, L. (1953) Wave Propagation in Periodic Structures, Electric Filters and Crystal Lattices, Second edition. Dover Publications, New York.

Chree, C. (1889) The equations of an isotropic elastic solid in polar and cylindrical coordinates, their solutions and applications. *Transactions of the Cambridge Philosophical Society*, **14**, 250–369.

Fung, Y. C. (1965) *Foundations of Solid Mechanics*. Prentice-Hall, Englewood Cliffs. New Jersey.

Graff, K. F. (1975) *Wave Motion in Elastic Solids*. Ohio State University Press, Ohio.

Hughes, T. J. R. (1987) *The Finite Element Method, Linear Static and Dynamic Finite Element Analysis*. Prentice-Hall, Englewood Cliffs, New Jersey.

Kohn, W., Krumhansl, J. A. and Lee, E. H. (1972) Variational methods for dispersion relations and elastic properties of composite materials. *ASME Journal of Applied Mechanics*, **39**, 327–336.

McNiven, H. D., Sackman, J. L., and Shah, A. H. (1963) Dispersion of axially symmetric waves in composite elastic rods. *Journal of the Acoustical Society of America*, **35**, 1602–1609.

Meitzler, A. H. (1965) Backward-wave transmission of stress pulses in elastic cylinders and plates. *Journal of the Acoustical Society of America*, **38**, 835–842.

Mindlin, R. D. and Herrmann, G. (1951) A one-dimensional theory of compressional waves in an elastic rod. In *Proceedings of the* 1*st U.S. National Congress of Applied Mechanics*. ASME. New York, pp. 187–191.

Murakami, H. and Akiyama, A. (1985) A mixture theory for wave propagation in angle-ply laminates, part 2: application. *ASME Journal of Applied Mechanics*, **52,** 338–344.
Murakami, H. and Yamakawa, J. (1997) Development of one dimensional models for elastic waves in heterogeneous beams. *ASME Journal of Applied Mechanics* (in preparation).
Nelson, R. B., Dong, S. B. and Kalra, R. D. (1971) Vibration and waves in laminated orthotropic circular cylinders. *Journal of Sound and Vibration*, **18,** 429–444.
Noble, B. and Daniel, J. W. (1977) *Applied Linear Algebra*. Prentice-Hall, Englewood Cliffs, New Jersey, Chapter 9.
Onoe, M., McNiven, H. D. and Mindlin, R. D. (1962) Dispersion of axially symmetric waves in elastic rods. *ASME Journal of Applied Mechanics*, **29,** 729–734.
Pao, Y.-H. and Mindlin, R. D. (1960) Dispersion of flexural waves in an elastic circular cylinder. *ASME Journal of Applied Mechanics*, **27,** 513–520.
Pochhammer, L. (1876) Uber die fortpflanzungsgeschwindigkeiten kleiner schwingungen in einem unbegrenzten isotropen kreiszylinder. *Zeitschrift fur Reine und Angewandte Mathematik*, **81,** 324–336.
Rattanawangcharoen, N., Shah, A. H. and Datta, S. K. (1992) Wave propagation in laminated composite circular cylinders. *International Journal of Solids and Structures*, **29,** 767–781.
Shimizu Corporation (1995) *Report on the* 1995 *Hyogoken-Nanbu Earthquake* (in Japanese). Tokyo, Japan.

APPENDIX A: BASIC EQUATIONS FOR THE FE IMPLEMENTATION

A typical finite element region $\Gamma^{(e)}$ is defined by a coordinate map from the standard cubical region in the ξ, η, ζ-space, $|\xi| \leqslant 1$, $|\eta| \leqslant 1$, $|\zeta| \leqslant 1$. The corner points are identified by element nodes, 1 to 8, in the counterclockwise direction with respect to the ζ-axis. These nodal coordinates in the cubical region are, from node 1, 2, 3, ..., and 8, in this order, $(-1, -1, -1)$, $(1, -1, -1)$, $(1, 1, -1)$, ..., $(-1, 1, 1)$. For notational convenience, node numbers are denoted by hatted integers, $\hat{i} = 1$–8. The shape functions, employed for both coordinate and displacement mappings, are defined as:

$$N_{\hat{i}} = \tfrac{1}{8}(1+\xi_{\hat{i}}\xi)(1+\eta_{\hat{i}}\eta)(1+\zeta_{\hat{i}}\zeta), \tag{A1}$$

where

$$(\xi_{\hat{i}}, \eta_{\hat{i}}, \zeta_{\hat{i}}), \quad \hat{i} = 1-8,$$

are the nodal coordinates, defined in the above.

The displacement field in $\Gamma^{(e)}$ is approximated by the nodal displacement vector $\{\hat{U}\}$,

$$\{u\} = [N]\{\hat{U}\} = \sum_{\hat{i}=1}^{8} \begin{bmatrix} N_{\hat{i}} & 0 & 0 \\ 0 & N_{\hat{i}} & 0 \\ 0 & 0 & N_{\hat{i}} \end{bmatrix} \begin{Bmatrix} \hat{U}_1^{\hat{i}} \\ \hat{U}_2^{\hat{i}} \\ \hat{U}_3^{\hat{i}} \end{Bmatrix}, \tag{A2}$$

where $\hat{U}_j^{\hat{i}}$ is the j th displacement component at node $\hat{i}$, and $[N]$ is the 3×24 interpolation matrix.

The strain-displacement matrix is defined as:

$$\{\varepsilon\} = [B]\{\hat{U}\}$$
$$= \sum_{\hat{i}=1}^{8} \begin{bmatrix} N_{\hat{i},1} & 0 & 0 \\ 0 & N_{\hat{i},2} & 0 \\ 0 & 0 & N_{\hat{i},3}+\sqrt{-1}kN_{\hat{i}} \\ 0 & N_{\hat{i},3}+\sqrt{-1}kN_{\hat{i}} & N_{\hat{i},2} \\ N_{\hat{i},3}+\sqrt{-1}kN_{\hat{i}} & 0 & N_{\hat{i},1} \\ N_{\hat{i},2} & N_{\hat{i},1} & 0 \end{bmatrix} \begin{Bmatrix} \hat{U}_1^{\hat{i}} \\ \hat{U}_2^{\hat{i}} \\ \hat{U}_3^{\hat{i}} \end{Bmatrix}. \tag{A3}$$

The elastic modulus matrix is defined for isotropic materials as:

$$[D] = \frac{E}{(1+\nu)(1-2\nu)} \begin{bmatrix} 1-\nu & \nu & \nu & 0 & 0 & 0 \\ \nu & 1-\nu & \nu & 0 & 0 & 0 \\ \nu & \nu & 1-\nu & 0 & 0 & 0 \\ 0 & 0 & 0 & \dfrac{1-2\nu}{2} & 0 & 0 \\ 0 & 0 & 0 & 0 & \dfrac{1-2\nu}{2} & 0 \\ 0 & 0 & 0 & 0 & 0 & \dfrac{1-2\nu}{2} \end{bmatrix}. \tag{A4}$$

APPENDIX B: DISPERSION SPECTRA OF ELEMENTARY THEORIES

Let the average displacements of each cross sectional plane be denoted by U_i (x_3, ω). The axial force is denoted by N_3, and the bending moments with respect to the x_1- and x_2-axes are M_1 and M_2, respectively.

Rayleigh's beam equations and the rod equation in the frequency domain become (Fung, 1965, Chapter 11):

$$-M_{2,33}+\omega^2(mU_1-J_2U_{1,33})=0, \tag{B1}$$

$$M_{1,33}+\omega^2(mU_2-J_1U_{2,33})=0, \tag{B2}$$

$$N_{3,3}+\omega^2 mU_3=0, \tag{B3}$$

where m is mass per unit axial length, and J_1 and J_2 are mass moments of inertia. These quantities are defined by the integral over the cross sectional region W at $x_3 = h/2$ as:

$$[mJ_1\ J_2]=\iint_W \rho[1\ x_2^2\ x_1^2]\,dx_1\,dx_2. \tag{B4}$$

Equations (B1) and (B2) describe the bending deformation in the x_1,x_3- and x_2,x_3-planes, respectively, while (B3) describes the longitudinal deformation of the rods. If the rotatory inertia terms, represented by J_1 and J_2 in (B1) and (B2), are neglected, the Euler-Bernoulli beam equations are recovered.

The associated constitutive relations are

$$N_3=(EA)_{(m)}U_{3,3}, \tag{B5}$$

$$M_1=-(EI_1)_{(m)}U_{2,33}, \tag{B6}$$

$$M_2=(EI_2)_{(m)}U_{1,33}, \tag{B7}$$

where the overall moduli are defined as:

$$[(EA)_{(m)}(EI_1)_{(m)}(EI_2)_{(m)}]=\iint_W E[1\ x_2^2\ x_1^2]\,dx_1\,dx_2. \tag{B8}$$

The equations of motion, (B1)–(B3), are rewritten in terms of displacements by substituting (B5)–(B7).

To obtain phase velocity spectra from (21a), a harmonic wave form in the x_3-direction is assumed:

$$[U_1\ U_2\ U_3]=[\tilde{U}_1\ \tilde{U}_2\ \tilde{U}_3]\exp(\sqrt{-1}kx_3). \tag{B9}$$

The substitution of (B9) into the equations of motion for displacements furnishes

$$[-k^4(EI_2)_{(m)}+\omega^2(m+k^2J_2)]\tilde{U}_1=0, \tag{B10}$$

$$[-k^4(EI_1)_{(m)}+\omega^2(m+k^2J_1)]\tilde{U}_2=0, \tag{B11}$$

$$[-k^2(EA)_{(m)}+m\omega^2]\tilde{U}_3=0. \tag{B12}$$

For a nontrivial amplitude, $\tilde{U}_i$, the phase velocity becomes for flexural motion in the x_1,x_3-plane,

$$C_p=k\sqrt{\frac{(EI_2)_{(m)}}{m+k^2J_2}}, \tag{B13}$$

for flexural motion in the x_2,x_3-plane,

$$C_p=k\sqrt{\frac{(EI_1)_{(m)}}{m+k^2J_1}}, \tag{B14}$$

and for longitudinal motion,

$$C_p=\sqrt{\frac{(EA)_{(m)}}{m}}. \tag{B15}$$

For longitudinal wave motion, the elementary theories predict a nondispersive phase velocity, (B15), independent of k.